Springer

KSME

Journal of Mechanical Science and Technology 26 (2) (2012) 495~508
www.springerlink.com/content/1738-494x
DOI 10.1007/s12206-011-1033-4

Effects of preloads on joints on dynamic stiffness of a whole machine tool structure †

Liang MI*, Guo-fu YIN, Ming-nan SUN and Xiao-hu WANG

School of Manufacture Science and Engineering, Sichuan University, Chengdu 610065, China

(Manuscript Received January 21, 2011; Revised July 21, 2011; Accepted October 17, 2011)

Abstract

The machine tool joint is a very important factor in the overall machine tool dynamic analysis, and it has great effects on the machining performance of a machine tool. As a very important operation parameter, preload greatly influences the stiffness and the damping of a machine tool joint. This paper presents the effect of preload on the dynamic stiffness of the spindle nose of a horizontal machining center. By discussing types and distribution of machine tool joints, studies on the joints of ball screws, linear guides and bolts are carried out. The influence of preload on the axial stiffness of a ball screw is calculated based on Hertzian contact theory and the effect of pretightening moment on pressure of bolt joint is discussed, while the dynamic stiffness and the damping of a linear guide are identified by an optimum algorithm with the simulated and experimental results. A finite element model (FEM) of the whole machine tool structure considering the effects of different joints is created and verified against the test results, and then the influence of preloads on ball screws and linear guides is predicted. Results indicate that preloads on machine tool joints have significant effects on the dynamic stiffness of the spindle nose.

Keywords: Ball screw; Dynamic stiffness; Linear guide; Machining center; Natural frequency; Preload

1. Introduction

The dynamic performance of a machine tool is typically represented in terms of frequency response functions (FRFs) and stability lobe diagrams (SLDs) for chatter. They experimentally determine machining efficiency and quality [1]. Researches have been carried out to predict the FRF of spindle nose [2, 3]. Because other components also contribute much to the spindle nose dynamic stiffness, it is limited that we only study the spindle system [4-6]. Therefore it is necessary to create the dynamic model of the whole machine tool structure and predict its behavior.

A machine tool is a complicated system composed of many components with many joints. Its dynamic behavior is not only determined by these components but also by the dynamic characteristics of various joints. Researches of Zhang and Huang et al. show that about 60% of the total dynamic stiffness and about 90% of the total damping in a whole machine tool structure originates in the joints [7]. Therefore analysis of the dynamic behavior of a whole machine tool structure should be conducted in two ways: joints characteristics identification [8-14] and dynamic modeling of the whole machine tool structure.

Considering nonlinearities of the machine tool joints [8], Dhupia introduced a nonlinear receptance coupling approach (NLRCA) and analyzed the effects of a nonlinear joint on the dynamic performance of a machine tool [15]. He generated the SLD of an arch-type reconfigurable machine tool (RMT) including the effects of joint nonlinearity. To model the damping of machine tool, Neugebauer et al. demonstrated a theoretical state-space modeling of non-proportional damped mechanics using a biaxial vertical lathe [16]. To predict the dynamic behavior of a overall machine tool at the design stage, Zhang et al. established a model of the whole machine tool structure composed of elements such as distributed mass beam, lumped mass and joints. Based on the dynamic fundamental parameters of the joints, they set up the dynamic equations of the whole machine tool structure with the method of receptance synthesis. An example showed the model is accurate [7, 17]. Other researchers modeled the column-spindle system by finite element method in the commercial software ANSYS. Both experimental and simulated results showed that the linear guides greatly affect the vibration behavior of the spindle head [18].

Preload on joint is a very important operation parameter of the machine tool. Researches indicated that preload had great

† This paper was recommended for publication in revised form by Associate Editor Chang-Wan Kim

* Corresponding author. Tel.: +86 028 85400507
E-mail address: miliang1985@yahoo.com.cn

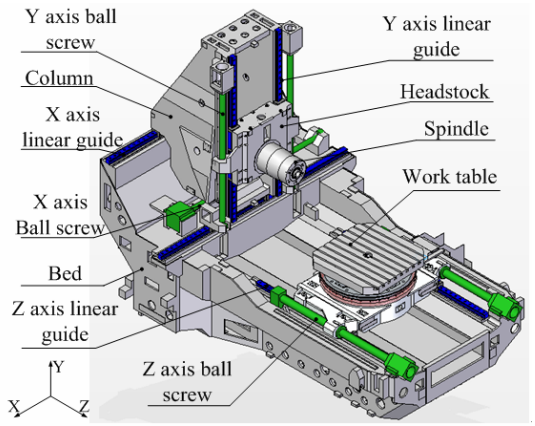

Fig. 1. Whole model of the horizontal machining center.

influences on the stiffness and the damping of machine tool joints [4, 5, 8, 9, 13, 17, 19]. The preload technology of the rolling bearing for the spindle of machine tools has been widely discussed in other researches [4, 5, 20, 21]. Variable preload control devices for a spindle rolling bearing were proposed based on centrifugal and electromagnetic forces [22, 23]. For the whole machine tool structure with bearings, linear guides, ball screws and bolt joints, it is important to analyze the relationship between the preloads on joints and the spindle nose dynamic stiffness. Clarifying the relationship is helpful in adopting reasonable preloads. This study aims at investigating the influences of preloads on linear guides and ball screws on the dynamic stiffness of the spindle nose of a horizontal machining center. For this, this paper discusses the types and distribution of different machine tool joints, proposes a finite element model of a horizontal machining center with the integration of the modeling of linear guides, ball screws and other joints. Experimental measurement results are introduced to modify and validate this FEM. With this FEM, dynamic stiffness of the spindle nose under different preloads is predicted. Results indicate that preloads on machine tool joints have significant effects on the dynamic stiffness of the spindle nose.

2. Whole machine tool structure and its joints

The whole machine tool structure of the horizontal machining center studied in this paper is mainly composed of the bed, the column, the headstock, the spindle and the work table as shown in Fig. 1. The size of the work table is 1×1 m. Travels in the X, Y, Z direction of the machining center are 1.7 m, 1.35 m and 1.4 m, respectively. Since the automatic tool changing system is positioned on the foundation apart from the main structure, it is not depicted in Fig. 1.

We can confirm that there are four types of joints of the machining center from Fig. 1 and current researches [1, 4-7, 15, 17, 24]. They are:

(1) Ball screw
(2) Linear guide
(3) Bolt joint

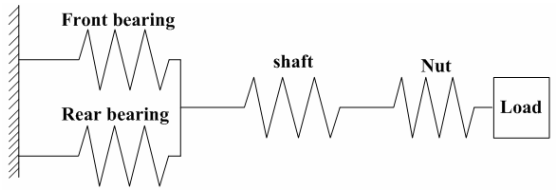

Fig. 2. Dynamic model of the ball screw.

(4) Bearing.

Since the stiffness of the bearings can be obtained from their manufacturer, we mainly focus on the dynamic characteristic identification of the ball screw, the linear guide and the bolt joint.

3. Interface characteristic identification of machine tool joints

3.1 Stiffness of the ball screw

Ball screw is a commonly used feeding device of machine tool which carries the major load in the feeding direction. Hence predicting the dynamic behavior of the whole structure should focus on the axial stiffness of the ball screw [24, 25].

The dynamic model of the ball screw is shown in Fig. 2. The axial stiffness of the ball screw can be expressed as Eq. (1).

$$k_{BS} = \frac{1}{1/k_{shaft} + 1/k_{nut} + 1/k_{bearing}} \tag{1}$$

where k_{shaft} represents the axial stiffness of the screw shaft, k_{nut} is the axial contact stiffness of the interface between the screw shaft and the nut, $k_{bearing}$ refers to the axial stiffness of the ball screw support units.

In the FEM of the ball screw, the screw shaft and the nut are modeled with solid elements; the deformation effect of the ball screw support unit and the interface between the screw shaft and the nut are modeled with spring elements. The ball screw support unit stiffness was obtained from its manufacturer [26]. The contact stiffness of the interface between the screw shaft and the nut can be figure out as follow steps.

(1) Hertzian expression for contact deformation

For the ball screw, the contact stiffness of the interface between the screw shaft and the nut can be related to the local deformation at the point where rolling ball and raceway contact. By using the Hertz contact theory, the deformation can be expressed as:

$$\delta = kQ^{2/3} \tag{2}$$

where Q denotes the contact force and k represents the Hertz constant, which is determined from the material and geometry properties of the rolling ball and the raceway [24, 25, 27].

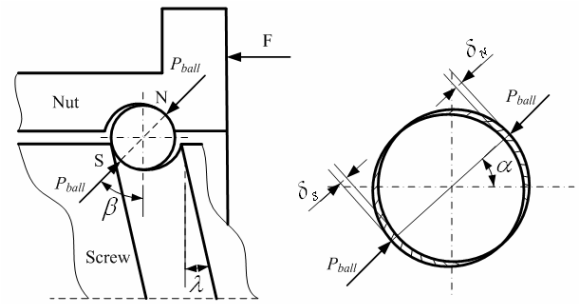

(a) The force acting on the ball screw (b) The force acting on the screw ball

Fig. 3. Loading conditions of ball screw.

(2) Ball screw axial stiffness without preload

Assume that the contact forces on each ball of the ball screw are equal when the ball screw is under load F. The loading conditions of the ball screw are shown in Fig. 3. The equilibrium condition of the ball screw is shown in Eq. (3).

$$F = zP_{ball}\sin\beta\cos\lambda \tag{3}$$

where P_{ball} is the contact force of each ball, β is the contact angle, λ is the helix angle, z is number of the balls and

$$z = i\pi d_0 / d_b \tag{4}$$

where i is the number of circuits, d_0 is the nominal diameter of the ball screw and d_b is the ball diameter.

The deformation conditions of each ball are shown in Fig. 3(b), and the total deformation is

$$\delta_T = \delta_S + \delta_N \tag{5}$$

where δ_S and δ_N are deformation between the rolling ball and the raceway of nut and the screw shaft respectively. They can be obtained from Eqs. (2) and (3) combined.

$$\delta_{axial} = \frac{\cos\lambda}{\sin\beta}\delta \tag{6}$$

Thus, the axial stiffness of the ball screw without preload is

$$K = \partial F / \partial \delta_{axial} \ . \tag{7}$$

(3) Ball screw axial stiffness with preload

Generally, preload is used to enhance the carrying capacity of a ball screw. Research of NSK indicates the axial stiffness of a ball screw with preload is 2.8 times of that without preload on average [26]. The loading conditions of the ball screw with preload are shown in Fig. 4.

Assume the preload and the load are F_p, F, respectively, and the normal contact forces between the raceway and each ball of nut A and B are P_A and P_B. The equilibrium condition of the ball screw is given in Eq. (8).

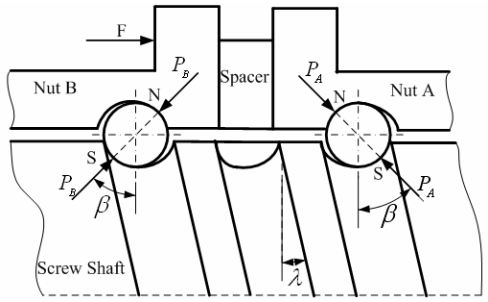

Fig. 4. Load conditions of the ball screw.

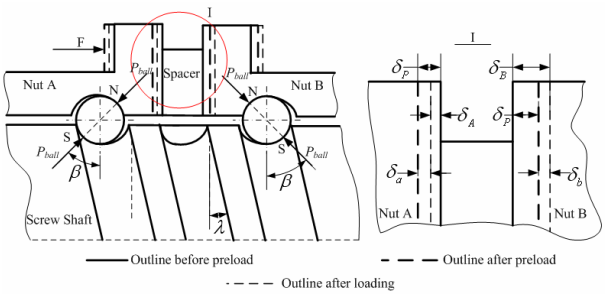

Fig. 5. Deformation of the ball screw.

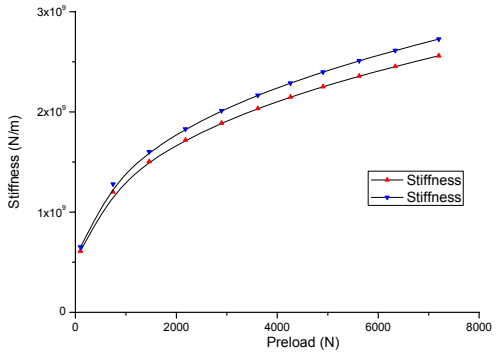

Fig. 6. The influence of preload on the axial stiffness of ball screw.

$$P_A z\sin\beta\cos\lambda - P_B z\sin\beta\cos\lambda - F = 0 \tag{8}$$

After preloading, the axial deformations of nut A and B are both δ_P. When load is applied, they change to δ_A and δ_B respectively. Assume that the axial deformation of nut A and B has changed δ_a, δ_b, respectively, then the compatibility conditions are

$$\delta_a = \delta_b \ . \tag{9}$$

Referring to Fig. 5, Eq. (9) can be written as

$$\delta_P - \delta_A = \delta_B - \delta_P \ . \tag{10}$$

The axial stiffness of the ball screw with preload can be obtained from Eqs. (3), (7), (8), (9), and (10) combined.

Table 1. Ball screw parameters.

Nominal diameter d_0 /mm	Ball diameter d_b /mm	Travel P_h /mm	Contact angle β / (°)	Form factor t	Preload P /kN	Rows × turns
50	7.9	20	45	0.52	2.68	1×3.8
55	7.9	20	45	0.52	2.68	1×3.8

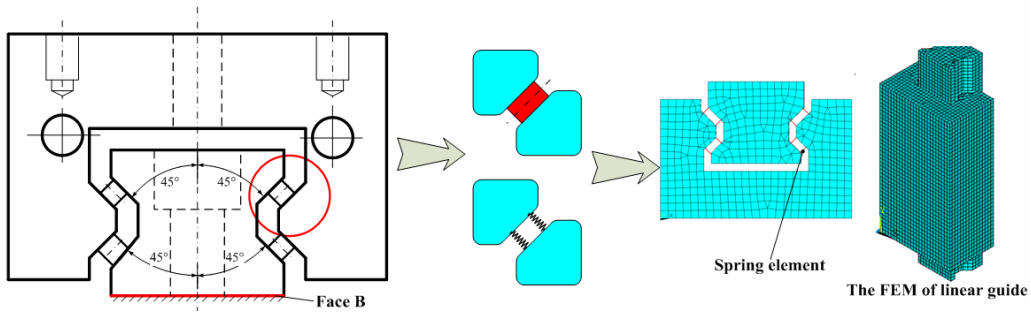

Fig. 7. Modeling of the linear guide.

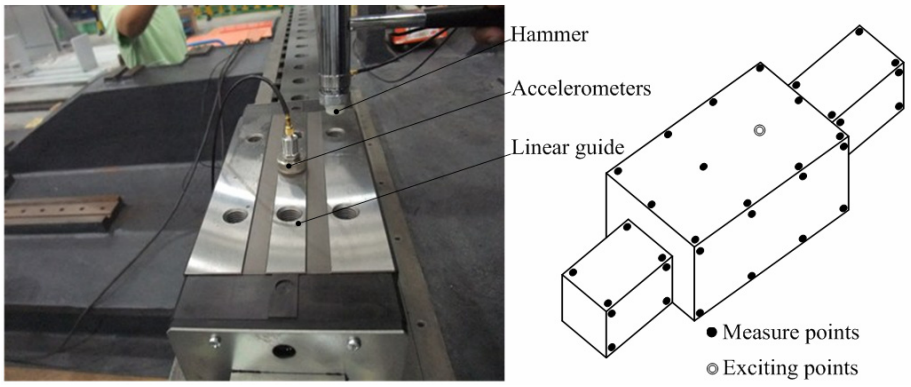

(a) Configuration of vibration test (b) Distribution of measure points

Fig. 8. Configuration of vibration test.

Basic parameters of the ball screw studied are listed in Table 1. Fig. 6 shows the change of axial stiffness of two types of ball screw under different preloads.

3.2 Interface dynamic characteristics identification of the linear guide.

The dynamic stiffness and the damping of the linear guide can be identified by combining the finite element analysis and the experimental results. The identification process is as follows.

A finite element model of the linear guide is created in the first place. The linear guide consists of a rail, a block and several rollers. The carriage and the rail is made of alloy steel, whose elastic modulus E = 2.06×10^{11} Pa, density ρ = 7850 kg/m^3 and Poisson's ratio μ=0.3. To build the FEM, we meshed the carriage and the rail with brick elements. And we chose the spring elements to simulate the stiffness and damping of the linear guide interfaces.

Ignoring the mass of the rollers, we used 72 spring elements to connect the block and the guide, which is demonstrated in Fig. 7. By using the finite element modal analysis with estimated stiffness coefficients, the ranges of natural frequencies and vibration mode shapes are predicted.

A modal test was carried out to measure the natural frequencies, damping ratios and vibration mode shapes. The experiment was implemented with multiple inputs to obtain a single output. This means that an accelerometer is set on a special point and the actuator excites a group of points to find out the FRF of each input point and the output point. As shown in Fig. 8(a), the linear guide was fixed and the accelerometer was set on the center of the upper face of the block. Based on the results of the finite element model analysis and Ref. [14], the typical mode shapes are pitching, rolling, yawing and vertical motions. To better compare the simulated and measured results, we located the excitation points at the points that had the largest amplitudes in any one of the three directions due to the finite element modal analysis results.

Table 2.Comparison of the predicted and experimental frequencies.

	1	2	3	4	5
Measured (Hz)	955.6	1469	1598	1969	2286
Predicted (Hz)	1046.	1371	1726	1807	2150
Relative error (%)	9.53	6.63	8.01	8.10	5.96

Table 3. Comparison of the predicted and experimental damping ratios.

	1	2	3	4	5
Measured	1.487	1.6219	2.497	2.595	3.393
Predicted	1.399	1.5042	2.7623	2.8141	3.511
Relative error	5.92%	7.26%	10.6%	8.44%	3.48%

In the experiments, 44 different points either on the rail or on the block were excited in corresponding directions to obtain the FRF of each point as shown in Fig. 8(b). The accelerometer sensitivity was 100 mV/g, and an impulse hammer with a force sensor and white plastic tip was used to excite the guide. Acceleration signals and impact force signals recorded by the digital analyzer INV3020C were used by the DASP data processing system to calculate the FRFs. Then by adopting the ERA method of DASP, the natural frequencies, the damping ratios and the vibration mode shapes could be obtained. For the linear guide, the actual natural frequencies, damping ratios are shown in Tables 2 and 3.

Stiffness and damping coefficients are identified by using the optimum algorithm. The objective function can be given as

$$\min f_1(k) = \left[\sum_{j=1}^{m} \left(\frac{\omega_j(k) - \bar{\omega}_j}{\bar{\omega}_j} \right)^2 \right] \cdot \beta_l^2 , \quad (11)$$

$$\min f_2(c) = \left[\sum_{j=1}^{m} \left(\frac{\xi_j(c) - \bar{\xi}_j}{\bar{\xi}_j} \right)^2 \right] \cdot \beta_l^2 \quad (12)$$

where $\omega_j(k)$ and $\xi_j(c)$ are the jth natural frequency and damping ratio calculated from the FEM, as well as the functions of the design variables, $\bar{\omega}_j$ and $\bar{\xi}_j$ are the jth natural frequency and damping ratio measured by experiments, m is the number of fitted modes, j is the mode order, and β_l is the scale transformation coefficient of the objective functions.

Types and models of the linear guides set on this machine center are the same. We studied one of these linear guides in situations with high preload and low preload. The preload codes of linear guide with high preload and low preload are C0 and C1, respectively. The stiffness and the damping coefficients of the linear guide with high preload (C0) obtained by this method are 3.59×10^9 N/m and 2450 N·s/m. Fig. 9 shows the identifying process. The experimental and calculated results of natural frequencies and damping ratios of the linear guide are listed in Tables 2 and 3. Comparison of the experimental and calculated results shows that the FEM of the linear guide developed in this study can describe the dynamic characteristics of the linear guide with an acceptable accuracy. The stiffness and the damping coefficients obtained from this research are accurate enough for creating the FEM of the whole machine tool structure. The stiffness and the damping coefficients of the linear guide with low preload (C1) obtained by this method are 3.08×10^9 N/m and 2987 N·s/m. The stiffness and the damping coefficients of the linear guide with high and low preload reveal that the preload greatly increases the stiffness of the linear guide and decreases the damping coefficients of the linear guide simultaneously.

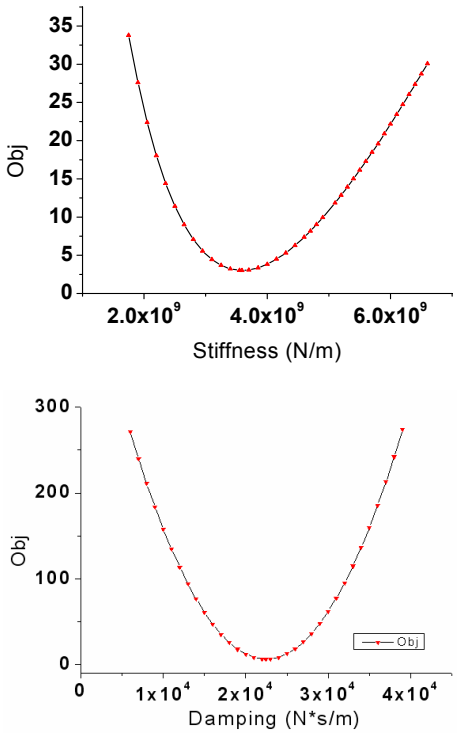

Fig. 9. The process of identifying interface characteristic of the rolling guide.

3.3 Dynamic interface characteristic of bolt joints.

A bolt joint is a typical kind of fixed joint which exists widely in the whole machine tool structure. Researches indicate that the dynamic characteristics of the bolt joint are determined by many factors, such as material, appearance, pressure, geometry shapes, etc. [7, 8, 13]. As one of the main factors, pressure is determined by the pre-tightening moment. The effect of pre-tightening moment is as follows:

A typical bolt joint as shown in Fig. 10(a) consists of part A, part B, a bolt and a nut. T is the tightening torque of bolt joint, $U_f$and F_p are the tangential and axial forces of the nut due to the tightening torque. The moment equilibrium condition of the nut is shown in Eq. (13).

$$T=T_p+T_f \quad (13)$$

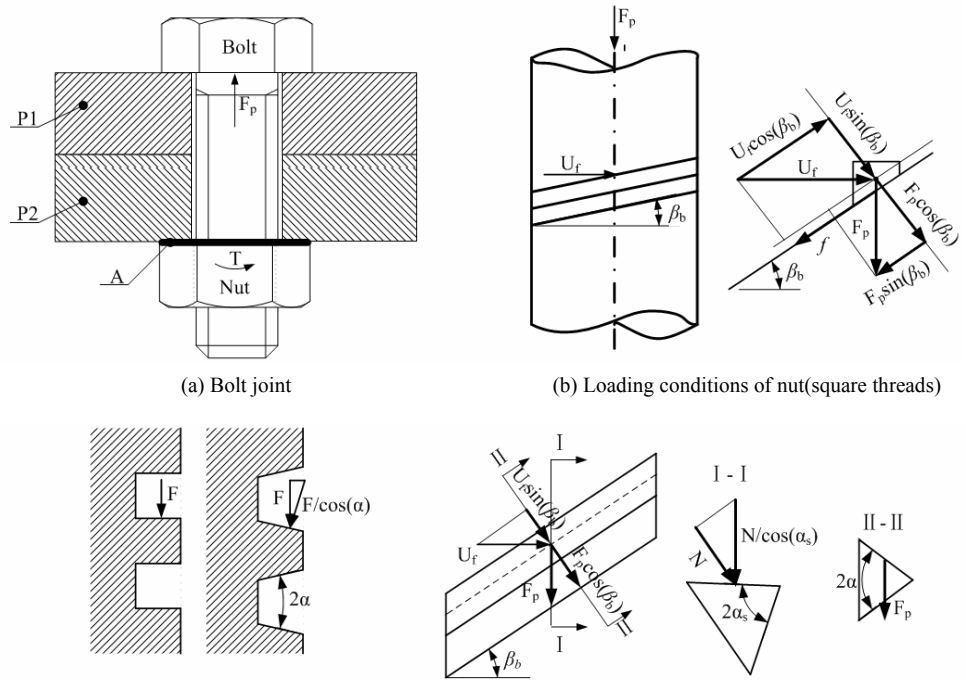

(a) Bolt joint (b) Loading conditions of nut(square threads)

(c) Comparison of standard threads and square threads (d) Loading conditions of nut(standard threads)

Fig. 10. Effects of pre-tightening moment.

where T is the tightening torque of bolt joint, T_p is the torque due to U_f, T_f is the frictional torque between face A (Fig. 10(a)) and the nut and

$$T_f = f r_n = r_n \mu_n F_p , \tag{14}$$

$$r_n = \frac{\left(D_1^3 - D_0^3\right)}{3\left(D_1^2 - D_0^2\right)} . \tag{15}$$

$$T_p = r_1 U_f \tag{16}$$

where μ_n is the friction coefficient between face A (Fig. 10(a)) and the nut, r_n is the equivalent frictional radius of the nut, D_0 is the pitch diameter of the thread hole, D_1 is the diameter of the nut.

For simplification, a square-threaded screw with a single thread is considered. The loading conditions of the nut are shown in Fig. 10(b). Thus we can conduct the equilibrium condition of the nut, as shown in Eq. (17).

$$U_f \cos(\beta_b) - F_p \sin(\beta_b) - f = 0 , \tag{17}$$

$$F = \mu(U_f \sin(\beta_b) + F_p \cos(\beta_b)) \tag{18}$$

where β_b is the lead angle, f is the friction force which acts opposite to the motion, μ is the friction coefficient between bolt and nut. Then,

$$U_f = F_p \frac{\mu + \tan(\beta_b)}{1 - \mu \tan(\beta_b)} . \tag{19}$$

Actually, the threads of most bolt joints are standard. The normal thread load is inclined to the axis because of the thread angle 2α and the lead angle β_b. The β_b can be neglected since it is very small, and only the effect of the thread angle is considered (Fig. 10(c)) [28]. The loading conditions are shown in Fig. 10(d), the angle α_s increases the frictional force by the wedging action of the threads. The friction force is obtained from Eq. (18), where the equation must be divided by $\cos(\alpha_s)$:

where β_b is the lead angle, f is the friction force which acts opposite to the motion, μ is the friction coefficient between bolt and nut. Then,

$$f = \mu(U_f \sin(\beta_b) + F_p \cos(\beta_b))/\cos(\alpha_s). \tag{20}$$

The effects of lead angle are neglected, and

$$\alpha = \alpha_s. \tag{21}$$

The tangential force of nut U_f can be obtained from Eq. (17) and Eq. (20) combined.

$$U_f = F_p \frac{\tan(\beta_b) - \mu/\cos(\alpha)}{1 - \tan(\beta_b)\mu/\cos(\alpha)} \tag{22}$$

The tightening torque T can be obtained from Eqs. (13), (14), (16) and (22) combined.

$$T = r_n \mu_n F_p + r_1 F_p \frac{\tan(\beta_b) - \mu/\cos(\alpha)}{1 - \tan(\beta_b)\mu/\cos(\alpha)} \tag{23}$$

Canceling $\tan(\beta_b)\mu/\cos(\alpha)$(which is small), the normal force of bolt joint is obtained:

$$F_p = \frac{T}{r_n\mu_n + r_1(\tan(\beta_b) - \mu/\cos(\alpha))}. \quad (24)$$

From the geometry conditions of bolt, the lead angle $\beta_b = P/2\pi r_1$ [29]. The pressure of bolt joint is

$$P_b = \frac{T}{\left(\frac{P}{2\pi} + \frac{\mu r_1}{\cos\beta} + \mu_n r_n\right)A} \quad (25)$$

where A is the area of bolt joint.

For a bolt joint with many bolts, we suppose the force of every bolt is equal, and this is accurate enough in engineering. The pressure of bolt joint is obtained from Eq. (25):

$$P_b = \frac{T}{\left(\frac{P}{2\pi} + \frac{\mu r_1}{\cos\beta} + \mu_n r_n\right)AN} \quad (26)$$

where N is the number of bolts.

The effects of pressure on the dynamic characteristics of bolt joint are complicated and have been widely discussed in other researches [7, 8, 13, 28, 29, 30]. These researches indicated the pressure's nonlinear effects on the contact stiffness and damping. The contact stiffness of bolt joint increases with the increase of pressure of bolt joint, but its rate decrease with the increase of pressure. The damping coefficient of a bolt joint decreases with the increase pressure of bolt joint, but its rate decreases with the increase of pressure. The reason might be determined by contact effect of joint.

In this paper, the dynamic characteristics of bolt joint under different pressure are obtained from Ref. [30].

4. Model creation and verification of the whole machine tool structure.

4.1 Vibration tests

The dynamic characteristics of the horizontal machining center mentioned in section 2 were obtained by measuring the direct frequency responses of accelerance of the whole structure at point A and the spindle nose. The device used for the vibration test consists of an accelerometer, a signal amplifier, an impact hammer, a digital analyzer INV3020C, DASP data processing system and a personal computer. The experimental setup is shown in Fig. 11. The accelerometer sensitivity is 100mV/g. Taking the working conditions of the machine tool into consideration, we focus on the dynamic characteristics between 0~500 Hz. An impulse hammer with a force sensor and rubber tip was used to excite the machine tool.

In the experiments, the exciting force produced by the impact hammer was applied in the X, Y direction of spindle nose and X direction of point A (Fig. 11). The acceleration signal and impact force signal are recorded by the digital analyzer INV3020C and FRFs are obtained with the help of the DASP system.

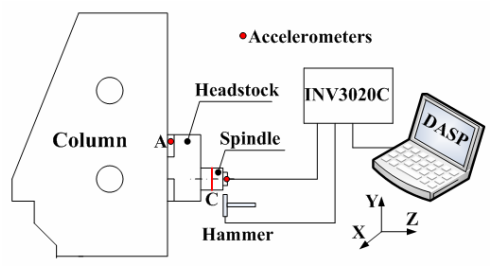

Fig. 11. Experimental setup of whole machine.

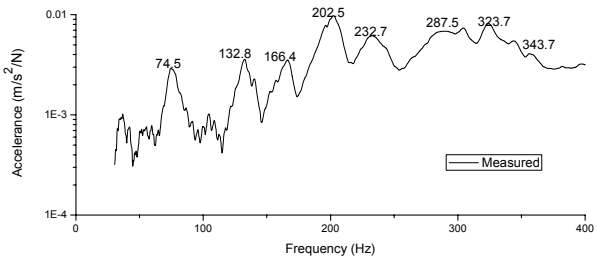

(a) A point

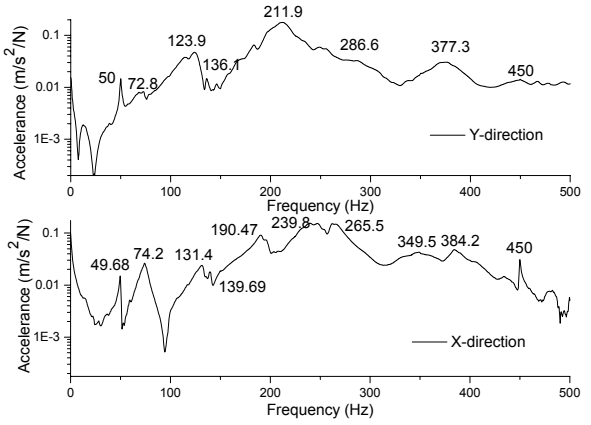

(b) Tool point

Fig. 12. Experimental frequency response of receptance.

The direct frequency responses of accelerance of the whole structure at point A and spindle nose are measured through exciting tests as shown in Fig. 12.

Comparing the two direct frequency responses of accelerance of the whole structure shown in Fig. 12(b), the FRF of the spindle nose in the X direction is obviously different with the FRF in the Y direction. As observed in Fig. 12, the FRF in the X direction exhibits a maximum accelerance of 0.1517 $m/s^2/N$ at frequency 239.8 Hz and the FRF in Y direction exhibits a maximum accelerance of 0.177 $m/s^2/N$ at frequency 211.9 Hz. But there are also connections between the two FRFs. For example, under the effect of the mode at 50 Hz frequency which mode shape is bending vibration of the col-

Table 4. Comparison of elements numbers between free meshing and hex meshing.

	Bed	Column	Spindle	Headstock	Work table
Hex meshing	45371	23788	3120	7938	8300
Free meshing	194042	48162	6831	13017	28014

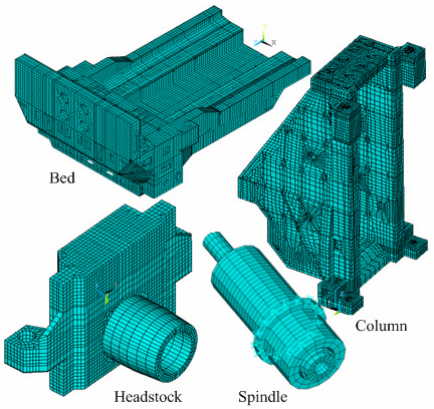

Fig. 13. FEMs of the parts.

umn along X-Y plane (Fig. 16(a)), there is a peak in X and Y direction FRF at 50 Hz frequency.

4.2 FEM of the whole machine tool structure

(1) FEMs of parts

The FEMs of parts are needed to create the FEM of the whole structure. Because of the complexity and large volume of the machine tool, free meshing might lead to massive elements and long solving time. To solve this problem, we meshed each part of the machine tool with eight-node brick element with Hypermesh, which simplified the creation of the spring elements. Table 4 lists the element numbers of free meshing and hex meshing. The bed, column, headstock and work table are made of cast iron, whose elastic modulus E = 1.3×10^{11} Pa, density ρ = 7250 kg/m3 and Poisson's ratio μ = 0.3. The spindle system is made of steel, whose elastic modulus E = 2.06×10^{11} Pa, density ρ = 7850 kg/m3 and Poisson's ratio μ = 0.3. The FEMs of the parts are shown in Fig. 13.

(2) Simulation of the joint interfaces

The dynamic characteristics of the horizontal machining center are determined by dynamic characteristics of each part and the joint interfaces which connect all the parts together. For the FEM of whole machine to be realistic, the parts of machine tool were modeled as solid elements (Fig. 13) and the joint interfaces were simulated with spring elements which connected the parts of the machine tool.

As shown in Fig. 14(a) a typical drive system consists of all the typical joints of the whole machine such as ball screw, bearing and linear guide [31] is proposed to indicate the simulation of joint interfaces.

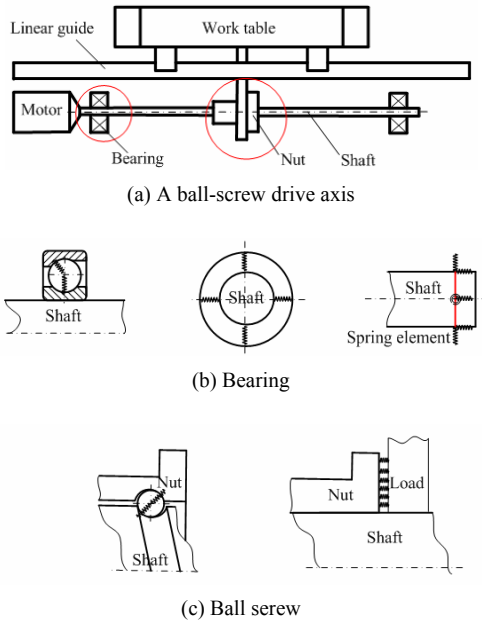

(a) A ball-screw drive axis

(b) Bearing

(c) Ball serew

Fig. 14. Simulation of joint interfaces.

Linear guide: In the finite element model of the whole machine tool structure, the finite element model of linear guide is shown in Fig. 7.

Bearing: The stiffness of bearing can be related to the local deformation at the points where rolling ball and raceway contact. To avoid the complexity in mesh generation, the mass of the outer ring, inner ring and rolling balls is ignored. Two types of four spring elements were created around the shaft to simulate axial and radial stiffness of the bearing, respectively (shown in Fig. 14(b)).

Ball screw: The shaft and the nut of ball screw are made of steel, whose elastic modulus $E = 2.06\times10^{11}$ pa, density ρ = 7850 kg/m^3 and Poisson's ratio $\mu = 0.3$. For simplification, the mass of the rolling balls is ignored and the shaft of the ball screw is modeled as a cylindrical shaft [18, 32]. The shaft and nut are meshed with brick elements. From the explanation of section 3.1, the axial stiffness of the ball screw can be related to the local deformation at the points where rolling ball and raceway contact. To simplify modeling, the nuts and shaft of ball screw were bonded together and the spring elements connecting the nut and the load (work table) were created to simulate he axial stiffness of the ball screw.

(3) FEM of the whole machine tool structure

The basic parameters of ball screws, bolt joints and bearings of the horizontal machining center are listed in Table 1, Table 5 and Table 6. The FEM of every part was used to assemble the FEM of the whole machine tool structure and spring elements were created to simulate the dynamic characteristics of joints interfaces as Fig. 14 shown. For the model to be realistic, the degrees of freedom of the nodes (translations in the x, y, and z directions) where machine tool fixed on ground were

Table 5. Bolt joints parameters.

Name	Material	Rough degree	Pressure (MPa)	Normal		Tangential	
				Stiffness (N/m)	Damp (N·s/m)	Stiffness (N/m)	Damp (N·s/m)
Face B (Fig. 7)	Cast iron-Steel	1.6	4.69	5.76×10^{11}	3.59×10^{7}	9.125×10^{10}	4.53×10^{6}
Face C (Fig. 11)	Cast iron-Steel	1.6	3.62	1.186×10^{11}	7.135×10^{6}	3.92×10^{10}	5.68×10^{6}

Table 6. Bearings parameters.

	Outer diameter *D*/mm	Inner diameter *d*/mm	Width *B*/mm	Contact angle *β*	Preload *P*/N	Stiffness of bearing sets	
						Axial ka/N/m	Radial kr/N/m
7022C	170	110	28	15	1770	2.03×10^{8}	1.015×10^{9}
7024C	180	120	28	15	1960	3.33×10^{8}	1.7325×10^{9}
40TAC90B	40	90	20	60	C9	1.015×10^{9}	—
45TAC100B	45	100	20	60	C9	1.16×10^{9}	—
50TAC100B	50	100	20	60	C9	1.745×10^{9}	—

Table 7.Vibration frequencies associated with mode shape of whole machine (unit: Hz).

Mode shape	Preload					
	Linear guide	Ball screw	Linear guide	Ball screw	Linear guide	Ball screw
	C0	100 KN	C1	2.68 N	C0	2.68 KN
Bending vibration of column along X–Y plane	48.7		45.5		49.1	
Torsion vibration of column about Y-axis	127.8		124.8		130.9	
Motion vibration of spindle along Z axis	187.1		186.2		201.3	
Torsion vibration of headstock about Z-axis	333		327.8		334.3	

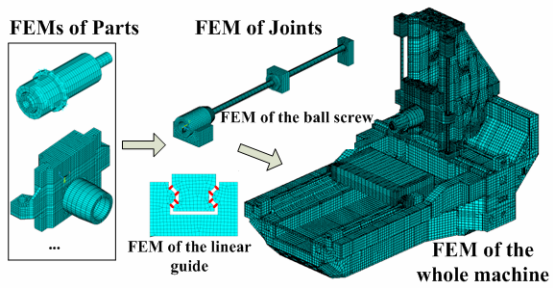

Fig. 15. Modeling of the whole machine.

constrained. By integrating these parameters and FEMs of each part, the FEM of the whole structure can be created as Fig. 15 shows.

4.3 Finite element analysis of whole machine tool structure

When the FEM was completed with acceptable accuracy, a modal analysis was performed to predict the natural frequencies and mode shapes of the whole structure. The vibration modes indicate the inherent vibration behavior of the machine responding to the external excitation and the relative displacement between different parts or modules, revealing the weak point of the whole structure. The fundamental vibration mode shapes of the whole machine tool are graphically depicted in Fig. 16, and the corresponding frequencies of these modes are list in Table 7.

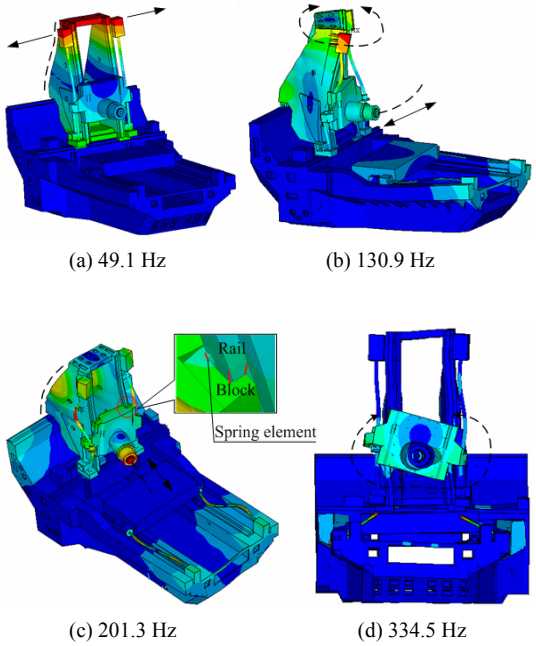

(a) 49.1 Hz (b) 130.9 Hz

(c) 201.3 Hz (d) 334.5 Hz

Fig. 16. Modal shapes of machine tool obtained from FEM.

As observed in Fig. 16, the first mode is the bending vibra-

Table 8. Comparison between the predicted and experimental natural frequencies of the whole machine. (unit: Hz).

Orders	1	2	3	4	5	6	7	8	9	10
Measured results	49.68	74.2	123.9	139.6	190.4	213.5	239.8	265.5	349.4	384.2
Predicted results	49.1	67.2	132.6	153	199.1	211.9	236.3	272.3	318.7	362.9
Relative error (%)	1.16	9.43	7.02	9.59	0.57	0.75	1.5	2.56	8.79	5.54

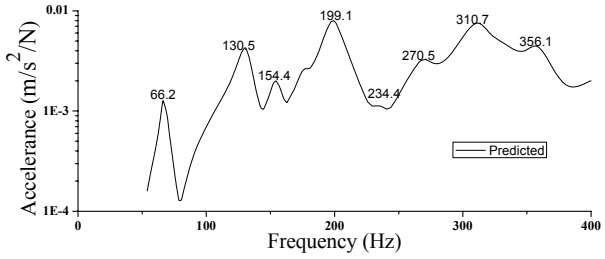

(a) Point A

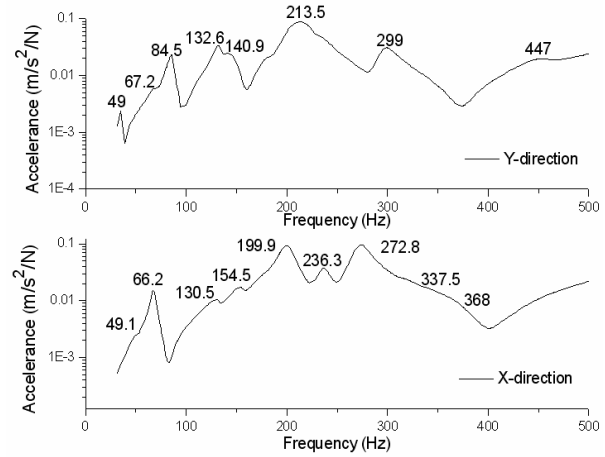

(b) Spindle nose

Fig. 17. Predicted frequency response of receptance.

tion of the column structure along the XY plane at frequency 49 Hz, and at frequency 130.9 Hz, the mode shape is the torsion vibration of column about Y-axis. These mode shapes are dominated by certain parts or modules. Other mode shapes exhibit relative motion between different parts or modules as Fig. 16(d) shows, which is torsion vibration of headstock about Z-axis.

The harmonic analysis is performed to calculate the FRFs of the whole structure. The direct frequency responses of accelerance of the whole structure at point and the spindle nose were predicted. And in this case, they are the same. The FRFs of these points are shown in Fig. 17.

Comparing the simulated and experimental results showed in Figs. 12 and 17, we can determine the accuracy of our model. Table 8 lists these results and their relative errors, from which we can see that the measurements agree well with the simulation based on the proposed model. To improve the accuracy of modeling, further work should concentrate on the joints nonlinearity and damping characteristics.

5. The influences of preloads on the dynamic characteristics of the whole machine tool structure.

5.1 The influences of preloads on the vibration modes

Modal analysis was performed with linear guide and ball screw under different preloads, and vibration frequencies of machine tool are summarized in Table 7. From comparisons of the results, the natural frequencies all rise due to the increase of the preloads, and the ranges vary from mode to mode. Since the mode shapes exhibit relative motion between different parts or modules, the effect of preload is more remarkable than those dominated by certain parts or modules. Considering the large volume of machine tool, the effect of preload is weak while the increase of natural frequency in Table 7 is less than 15 Hz.

5.2 The influences of preloads on the dynamic stiffness of spindle nose

The responding to the external excitation of machine tool is determined by the mode at the frequency of exciting force. The complication of preload effect on modes of the whole machine tool determines its complicated effects on dynamic stiffness of the spindle nose. Dynamic stiffness is usually used as a performance index for evaluating the mechanical characteristics of a machine tool structure; therefore, it is important to discuss the effect of preload on it. Harmonic response analysis, which is a technique used to determine the steady-state response of a linear structure to loads that vary sinusoidally with time, is performed to calculate the FRFs of the whole structure under unit force based on the FEM of the whole machine tool structure. The reciprocal of FRFs are dynamic stiffness of spindle nose.

Linear guide: With the linear guides in X, Y, Z directions under high (C0) and low (C1) preloads, the dynamic stiffness of the spindle nose in X, Y and Z directions is predicted and presented in Fig. 18. From Fig. 18, we can make these conclusions:

High preloads enhance the dynamic stiffness of the spindle nose. As we can see in Fig. 18(a), the minimum dynamic stiffness is 1.02×10^7 N/m at frequency 65.14 Hz under low preloads, while that is 1.18×10^7 N/m at frequency 67.28 Hz under high preloads. Since the machine center is much larger and heavier than the prototype of a vertical column – spindle, the influence of the linear guides is not as great as it is indicated by research [18].

The effects of preload of linear guide on the dynamic stiffness of spindle nose are complicated, in the following areas.

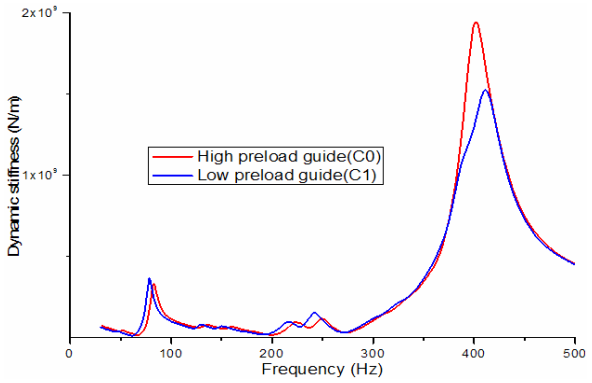

(a) X direction

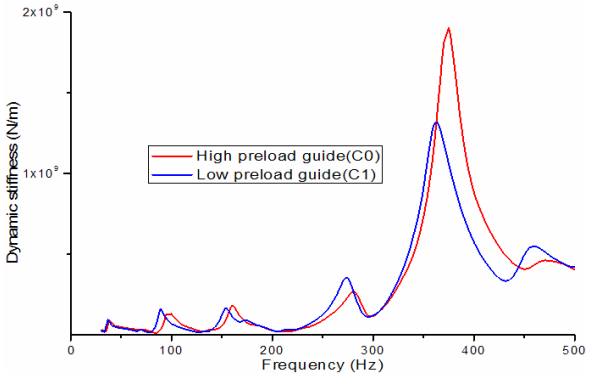

(b) Y direction

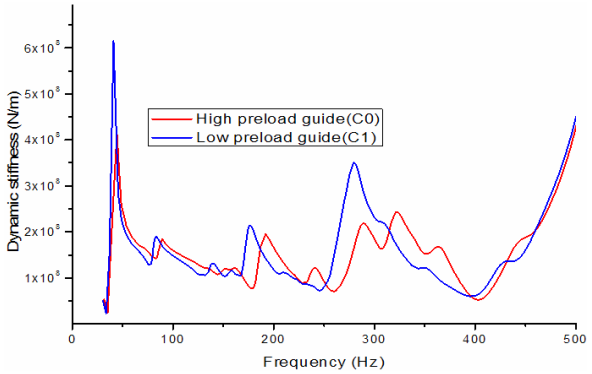

(c) Z direction

Fig. 18. The influence of linear guide preload.

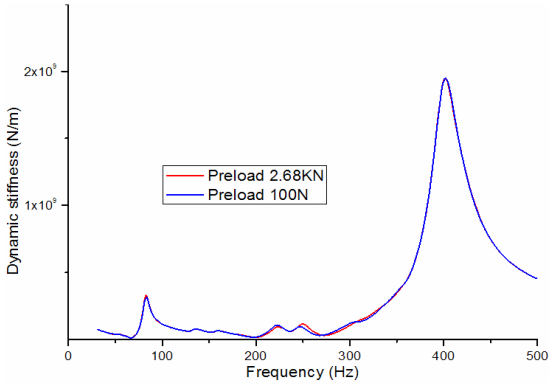

(a) X direction

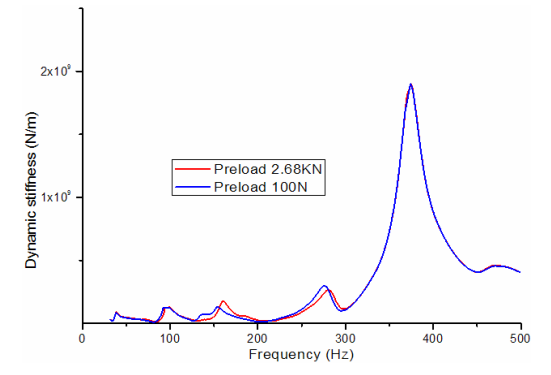

(b) Y direction

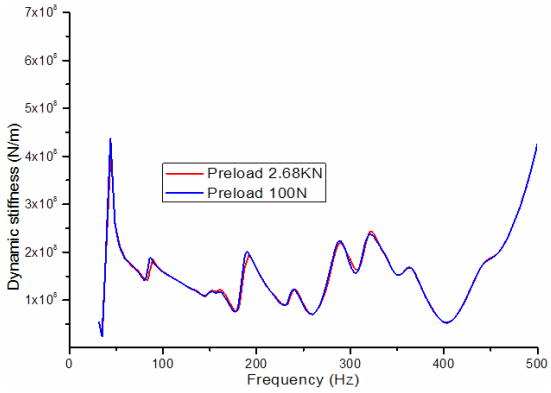

(c) Z direction

Fig. 19. The influence of ball screw preload.

(1) As the reason for difference of the dominate mode shapes at different frequencies, changes of preloads only influence the dynamic stiffness in several particular bands other than the whole one. For example, the dynamic stiffness almost remains the same from 0 Hz to 50 Hz in Fig. 18(b). The reason for this is that vibration mode in this band is bending vibration of column along X–Y plane. On the other hand, the effects of preload are significant at the bands from 200 Hz to 300 Hz and 350 Hz to 450 Hz. Under the support of high preload linear guide, the dynamic stiffness increases in Y direction in the band 350 Hz~450 Hz. Being in diametrical opposition, the dynamic stiffness of the spindle nose decreases with the rise of the preload of the linear guide from C1 to C0. This appears to go against the thinking about the effect of linear guide preload. The reason for this may be that the low preload linear guide has become a dynamic absorber of the machine tool. The "dynamic absorber effect" results in local increases of dynamic stiffness, and the same phenomenon is found in other joints in different directions of this machine tool and Refs. [2, 18]. Future researches will focus on the reasons for this effect.

(2) The effects of preload of linear guide on the dynamic stiffness of spindle nose in different directions are different at the same frequency. For example, when the preload of the

linear guide increases, the dynamic stiffness increases remarkably in the Z direction while remaining almost unchanged in X and Y directions at frequency 200 Hz. The reason for this is that the dominant mode shape at frequency 200 Hz is the motion vibration of headstock along the Z axis as Fig. 16(c) shows. The stiffness of the spindle in the Z direction and the stiffness of spring elements which is used to simulate the linear guide connecting the column and headstock are a connection in series. The increase of preload results in the increase of natural frequency and dynamic stiffness in the Z direction.

Ball screws: The dynamic stiffness of the spindle nose is depicted in Fig. 19 when the ball screws in X, Y, Z directions are under respective preloads of 100 N and 2.68 KN. Conclusions on the effects of preloads on ball screws are similar to that on the effects of preloads on linear guides, but there are also some specialties.

(1) In general, bands affected by ball screws are relatively narrower than that affected by linear guides. In the band from 120 Hz to 200 Hz and 250 Hz to 300 Hz in Fig. 19(b), however, the effect is great. This demonstrates that the motion vibration of spindle along Y axis is restricted by the axial stiffness of ball screws. As a result, the vibration frequencies at these bands are increased and the dynamic stiffness of the spindle nose is changed.

(2) The preloads on ball screws have bare effects on the dynamic stiffness in the Z direction of the spindle nose, which originates from the fact that the feeding movement in the Z direction is achieved by the work table other than by the spindle (Fig. 1). Therefore, the dynamic stiffness of the spindle nose in the Z direction is essentially affected by the stiffness of the spindle itself, rather than the ball screw.

6. Conclusions

This paper analyzes the effects of preloads on the dynamic stiffness of the spindle nose. With the analysis and results, we can draw the following conclusions:

(1) The influence of preloads on the axial stiffness of the ball screw is calculated base on the Hertz contact theory.

(2) The dynamic stiffness and the damping of linear guide are identified with the help of an optimum algorithm. Comparisons between the finite element analysis and the experimental results indicate that the model can reflect the dynamic characteristics of the linear guide accurately.

(3) The FEM of the whole machine tool structure considering the effects of joints is created and verified against the experimental results. This model can accurately simulate and predict the dynamic behavior of the machining center.

(4) Effects of various preloads on both linear guides and ball screws on the whole structure are studied. It turns out that preloads on the joints of the machining center have significant effects on the dynamic stiffness of the spindle nose. Preloads on different joints contribute quite differently to the dynamic stiffness in distinct bands of frequencies. At the same time, though increasing preloads can enhance the natural frequencies, it can also decrease the dynamic stiffness at some frequencies and thus deteriorate the dynamic performance of the machining center due to "dynamic absorber effect." Therefore, the preloads should be chosen reasonably during the design and manufacturing stage based on the customers' needs rather than simply increasing them.

Acknowledgment

This work is supported by the National Key Projects of Science and Technology of China, Grant No. 2010ZX04015-011 and Key Technology R&D Program of Chengdu, Grant 09RKYB980ZF-033. The authors are grateful to other participants of the projects for their cooperation.

Nomenclature

k_{BS} : Axial stiffness of the ball screw
k_{shaft} : Axial stiffness of the screw shaft
k_{nut} : Axial contact stiffness of the interface between the screw shaft and the nut
$k_{bearing}$: Axial stiffness of ball screw support unit
δ : Deformation at the contact point
Q : Contact force
k : Hertz constant, which is determined the material and geometry properties of rolling ball and raceway
P_{ball} : Contact force on each ball of the ball screw
β : Contact angle of the ball screw
λ : Helix angle of the ball screw
z : Number of balls
d_o : Nominal diameter of the ball screw
d_b : Ball diameter
i : Number of circuits
δ_T : Total deformation of each ball
δ_S, δ_N : Deformation between ball and the raceway of nut and screw shaft
δ_{axial} : Axial deformation of each ball
K : Axial stiffness of the ball screw without preload
F : Load on the ball screw
F_p : Preload on the ball screw
P_A, P_B : Normal contact forces between raceway and each ball of nut A and B
δ_P : Axial deformation of nut A and B after preloading
δ_A , δ_B : Axial deformation of nut A and B after loading
δ_a , δ_b : Changes of deformation of nut A and B after loading
P_h : Lead of the ball screw
t : Form factor of the ball screw
E : Elastic modulus
ρ : Material density
$\omega_j(k)$: jth natural frequency calculated
$\zeta_j(c)$: jth damping ratio calculated
$\overline{\omega}_j$: jth natural frequency measured
$\overline{\xi}_j$: jth damping ratio measured
m : Number of fitted modes

j : Mode order
β_l : Scale transformation coefficient of the objective functions
P_B : Pressure of bolt joints
T : Tightening torque of bolt joint
U_f, F_p : Tangential and axial force of nut due to tightening torque T
T_p : The torque due to U_f
T_f : Frictional torque between face A and nut
μ_n : Friction coefficient between face A and nut
r_n : The equivalent frictional radius of the nut
D_0 : Pitch diameter of thread hole
D_1 : Diameter of nut
β_b : Lead angle of bolt
f : Friction force which is acting opposite to the motion of nut
μ : Friction coefficient between bolt and nut
N : Number of bolts
P_b : Pressure of bolt joint
A : Area of bolt joint
P : Pitch of bolt

References

[1] J. Dhupia and B. Powalka et al., Dynamics of the arch-type reconfigurable machine tool, *International Journal of Machine tools & Manufacture*, 47 (2007) 326-334.

[2] T. L. Schmitz and M. A. Davies et al., Tool point frequency response prediction for high-speed machining by RCSA, *Transactions of the ASME, Journal of manufacturing science and engineering*, 123 (2001) 700-707.

[3] A. Ertürk and H. N. Ö Zgüven et al., Effect analysis of bearing and interface dynamics on tool point FRF for chatter stability in machine tools by using a new analytical model for spindle-tool assemblies, *International Journal of Machine Tools & Manufacture,* 47 (2007) 23-32.

[4] Y. Cao and Y. Altintas, A general method for the modeling of spindle bearing systems, *Transactions of the ASME, Journal of Mechanical Design,* 26 (2004) 1089-1104.

[5] Y. Cao and Y. Altintas, Modeling of spindle-bearing and machine tool systems for virtual simulation of milling operations, *International Journal of Machine Tools & Manufacturing,* 47 (2007) 1342-1350.

[6] P. Kolar and M. Sulitka et al., Simulation of dynamic properties of a spindle and tool system coupled with a machine tool frame, *International Journal of Advance Manufacture,* 54 (2011) 11-20.

[7] G. P. Zhang and Y. M. Huang et al., Predicting dynamic behaviours of a whole machine tool structure based on computer-aided engineering, *International Journal of Machine tools & Manufacture,* 43 (2003) 699-706.

[8] W. P. Fu, Y. M. Huang and G. P. Zhang, Experimental investigation on damping behavior of normal joint surface at unit area, *Modeling, Measurement and Control B, AMSE Press,* 51 (2) (1993) 13-20.

[9] K. Mao and B. Li et al., Stiffness influential factors-based dynamic modeling and its parameter identification method of fixed joints in machine tools, *International Journal of Machine tools & Manufacture*, 50 (2010) 156-164.

[10] Y. Lin and W. Chen, A method of identifying interface characteristic for machine tools design, *Journal of Sound and Vibration*, 3 (2002) 481-487.

[11] H. Y. Hwang, Identification techniques of structure connection parameters using frequency response function, *Journal of Sound and Vibration*, 212 (3) (1998) 469-479.

[12] T. Yang, S. -H. Fan and C. -S. Lin, Joint stiffness identification using FRF measurements, *Computer & Structures,* 81 (2003) 2549-2556.

[13] D. LI, Y. ZHANG and P. WANG, Dynamic model of machine joints based on structural damping (in Chinese), *Journal of Vibration and shock*, 29 (2010) 204-208.

[14] J. P. Hung, Load effect on the vibration characteristics of a stage with rolling guides, *Journal of Mechanical Science and Technology*, 23 (1) (2009) 92-102.

[15] J. S. Dhupia and B. Powalka et al., Effect of a nonlinear joint on the dynamic performance of a machine tool, *Journal of Manufacturing Science and Engineering*, 129 (2007) 943-950.

[16] R. Neugebauer and C. Scheffler et al., State space modeling of non-proportional passive damping in machine tools. *International Journal of Advance Manufacture,* 53 (2011) 945-952.

[17] G. ZHANG, W. SHI and Y. HUANG et al., Modeling and analysis method of dynamical characteristics for a whole machine tool structure (in Chinese), *Journal of Shanghai Jiao Tong University*, 35 (12) (2001) 1834-1837.

[18] C. Y. Lin, J. P. Hung et al., Effect of preload of linear guides on dynamic characteristics of a vertical column–spindle system, *International Journal of Machine Tools & Manufacture*, 50 (2010) 741-746.

[19] C. C. Wei, J. F. Lin et al., Analysis of a ball screw with a preload and lubrication, *Tribology International*, 42 (2009) 1816-1831.

[20] Y. -K. Hwang and C. -M. Lee, A review on the preload technology of the rolling bearing for the spindle of machine tools, *International Journal of Precision Engineering and Manufacture,* 11 (3) (2010) 491-498.

[21] S. Jiang, H. Mao, Investigation of variable optimum preload for a machine tool spindle, *International Journal of Machine Tools & Manufacturing*, 50 (2010) 19-28.

[22] Y. K. Hwang and C. M. Lee, Development of automatic variable preload device for spindle bearing by using centrifugal force, *International Journal of Machine Tools & Manufacturing*, 49 (2009) 781-787.

[23] Y. K. Hwang and C. M. Lee, Development of a newly structured variable preload control device for a spindle rolling bearing by using an electromagnet, *International Journal of Machine Tools & Manufacturing*, 50 (2010) 253-259.

[24] S. Jiang and S. Zhu, Dynamic characteristic parameters of linear guideway joint with ball screw (in Chinese), *Journal*

of Mechanical Engineering, 46 (2010) 92-99.
[25] C. WU, Study on axial contact stiffness of ball screws (in Chinese) [D], Changchun China, Jilin University, 2008.
[26] NSK, NSK bearing technical information, 2003.
[27] K. J. Johnson, *Contact mechanics*, Cambridge University Press, England (1985).
[28] D. B. Marghitu, *Mechanical engineer's handbook*, Academic Press, San Diego, USA (2001).
[29] J. Carvill, *Mechanical engineer's data handbook*, Butterworth-Heinemann, Burlington, USA (1993).
[30] B. Y. Liao, X. M. Zhou and Z. H. Yin, *Modern mechanical dynamics and its application: modeling, analysis, simulation, modification, control, optimization (in Chinese)*, China Machine Press, Beijing, China (2004).
[31] J. S. Chen, Y. K. Huang et al. Mechanical model and contouring analysis of high-speed ball-screw drive systems with compliance effect, *International Journal of Advance Manufacture,* 24 (2004) 241-250.
[32] C. E. Okwudire, Improved screw–nut interface model for high-performance ball screw drives, *Transactions of the ASME, Journal of Mechanical Design,* 133 (2011) 1009-1019.

Liang Mi received his B.S. in Mechanical Engineering from Sichuan University, China, in 2007. He is currently a Ph.D Student in the School of Manufacturing Science and Engineering, SCU. His research interests are CAE and machine tool dynamics.